# **RESEARCH ARTICLE**

Neural Circuits

# Synchronous spiking associated with prefrontal high $\gamma$ oscillations evokes a 5-Hz rhythmic modulation of spiking in locus coeruleus

<sup>⑤</sup> Nelson K. Totah, <sup>1,2,3</sup> Nikos K. Logothetis, <sup>1,4</sup> and <sup>⑤</sup> Oxana Eschenko¹

<sup>1</sup>Department of Physiology of Cognitive Processes, Max Planck Institute for Biological Cybernetics, Tübingen, Germany; <sup>2</sup>Helsinki Institute of Life Science, University of Helsinki, Helsinki, Finland; <sup>3</sup>Faculty of Pharmacy, University of Helsinki, Helsinki, Finland; and <sup>4</sup>Division of Imaging Science and Biomedical Engineering, University of Manchester, Manchester, United Kingdom

#### **Abstract**

The brainstem noradrenergic locus coeruleus (LC) is reciprocally connected with the prefrontal cortex (PFC). Coupling between LC spiking and the depolarizing phase of slow (1–2 Hz) waves in PFC field potentials during sleep and anesthesia suggests that LC drives cortical state transition. Reciprocal LC-PFC connectivity should also allow interactions in the opposing (top-down) direction, but prior work has only studied prefrontal control over LC activity using electrical or optogenetic stimulation. Here, we describe the physiological characteristics of spontaneously occurring top-down LC-PFC interactions. We recorded LC multiunit activity (MUA) simultaneously with PFC single-unit and local field potential (LFP) activity in urethane-anesthetized rats. We observed cross-regional coupling between the phase of 5-Hz oscillations in LC-MUA and the power of PFC LFP 60–200 Hz high  $\gamma$  (h $\gamma$ ). Transient increases in PFC h $\gamma$  power preceded peaks in the 5-Hz LC-MUA oscillation. Analysis of cross-regional transfer entropy demonstrated that the PFC h $\gamma$  transients were predictive of a transient increase in LC-MUA. An  $\sim$ 29 ms delay between these signals was consistent with the conduction velocity from the PFC to the LC. Finally, we showed that PFC h $\gamma$  transients are associated with synchronized spiking of a subset (27%) of PFC single units. Our data suggest that PFC h $\gamma$  transients may indicate the timing of the top-down excitatory input to LC, at least under conditions when LC neuronal population activity fluctuates rhythmically at 5 Hz. Synchronized PFC neuronal spiking that occurs during h $\gamma$  transients may provide a previously unknown mode of top-down control over the LC.

**NEW & NOTEWORTHY** The prefrontal cortex (PFC) is thought to control activity in the noradrenergic locus coeruleus (LC). Prior anatomical and prefrontal stimulation studies demonstrated the potential for PFC-LC interactions; however, it is unknown what types of PFC activity affect the LC. Here, we show that transient increases in PFC high  $\gamma$  power and associated changes in PFC unit-pair synchrony are a potential sign of top-down control over the LC.

 $\gamma$ ; locus coeruleus; synchrony;  $\theta$ ; top-down control

#### INTRODUCTION

A common assumption about coerulear-prefrontal [locus coeruleus-prefrontal cortex (LC-PFC)] functional connectivity is that the LC is a driver. This assumption is based on the well-documented actions of the LC as an ascending neuro-modulatory system (1–8). However, bidirectional LC-PFC interaction is also likely as LC and PFC are reciprocally and monosynaptically connected. Indeed, the PFC has been demonstrated to exert both inhibitory and excitatory effects

on LC activity (9–15). Notably, the PFC is the only cortical region sending direct projections to the LC (13, 15). Previous studies on LC-PFC interactions during sleep or anesthesia have focused on a prominent 1–2 Hz oscillation in LC spike rate that is thought to promote the transition to cortical heightened excitability (16–18). However, during urethane anesthesia, rhythmic LC activity occurs not only at  $\sim$ 1–2 Hz but also at  $\sim$ 5 Hz (17). Here, we studied the nature and the directionality of the LC-PFC interaction during these faster 5-Hz fluctuations of LC multiunit activity (MUA).



In the present study, we monitored LC-MUA and wideband extracellular activity from the prelimbic division of the prefrontal cortex (PFC) in urethane-anesthetized rats. Importantly, although recording LC-MUA for long durations and with stable spiking activity in behaving animals continues to present an immense challenge, anesthesia permits stable, long-lasting recordings to study physiological interactions between the LC and PFC. Here, we report cross-regional phase-amplitude coupling between LC-MUA 5-Hz oscillations and high  $\gamma$  (h $\gamma$ ; 60–200 Hz) LFP power in the PFC. Transient increases in PFC hγ power preceded LC-MUA 5-Hz oscillation peaks by a delay consistent with the known conduction velocity from the PFC to the LC. hy transients were associated with PFC unit-pair spike synchrony. Taken together, our results demonstrate that during epochs when LC population firing rate oscillates at 5 Hz,  $h\gamma$  transients may be a sign of PFC top-down excitatory control over the LC.

#### **MATERIALS AND METHODS**

#### **Subjects**

All experimental procedures were carried out with approval from the local authorities and in compliance with the German Law for the Protection of Animals in experimental research (Tierschutzversuchstierverordnung) and the European Community Guidelines for the Care and Use of Laboratory Animals (EU Directive 2010/63/EU). Male Sprague-Dawley rats (350–450 g) were used. Animals (specific-pathogen-free) were ordered from Charles River Laboratories (Sulzfeld, Germany). Animals were pair-housed and on a 0800 to 2000 dark to light cycle. Data were collected from rats used in a prior study (18).

#### **Anesthesia and Surgical Procedures**

Rats were anesthetized using an intraperitoneal (ip) injection of urethane at a dose of 1.5 g/kg body wt (Sigma-Aldrich, U2500). Oxygen was administered throughout the procedure and body temperature was maintained at 37°C using a heating pad and rectal probe to monitor body temperature. The skull was leveled to 0°, such that the difference between lambda and bregma was less than 0.2 mm.

### **Stereotaxic Coordinates and Electrode Placement**

Electrodes were targeted for the LC and the prelimbic cortex (PL). The coordinates for LC were 4.0 mm posterior from lambda, 1.2 mm lateral from lambda, and ∼6.0 mm ventral from the brain surface (implanted at a 15° posterior angle). The following coordinates, in relation to bregma and the brain surface, were used for PL: 3.0 mm anterior, 0.8 mm lateral, and 3.0 mm ventral.

The LC electrode was targeted based on standard electrophysiological criteria. These criteria included a slow spontaneous firing rate, biphasic response to noxious sensory stimuli (foot shock), audible presence of jaw movement-responsive cells in the mesencephalic nucleus of cranial nerve V with undetectable single units (<0.2 mV) from that structure. LC electrode placements were also verified using histological examination in 50-µm sections that were stained for cresyl violet or a 3,3'-diaminobenzidine (DAB) and horse radish peroxidase reaction with hydrogen peroxide to visualize

an antibody against tyrosine hydroxylase (the catecholamine synthesis enzyme).

#### **Electrodes**

The LC was recorded using either a single tungsten probe (FHC, Model UEWMFGSMCNNG) or a multichannel silicone probe (NeuroNexus, Model A1x32-Poly3-10mm-25s-177-A32). Deep-layer PFC LFP was recorded using a single tungsten probe (FHC). The impedance was 200–800 k $\Omega$ . For recordings of PFC single units, a Neuronexus A4x2-tet-5mm-500-400-312 probe was used. The probe was oriented running anterior-posterior in the deep layers.

# **Recording and Signal Acquisition**

A silver wire inserted into the neck muscle was used as a reference for the electrodes. Electrodes were connected to a preamplifier (in-house constructed) via low noise cables. Analog signals were amplified (by 2,000 for LC and 500 for cortex) and filtered [8 kHz low pass, direct current (DC) high pass] using an Alpha-Omega multichannel processor (Alpha-Omega, Model MPC Plus). Signals were then digitized at 24 kHz using a data acquisition device (CED, Model Power1401mkII).

#### Administration of Clonidine

At the end of the recording, a  $0.05\,\mathrm{mg/kg}$  dose of the  $\alpha$ -2 adrenergic agonist clonidine was injected intraperitoneally (Sigma-Aldrich, Product identification C7897). The recording was continued at least until LC activity ceased.

#### **Determination of Cortical State**

Cortical states were separated based on characteristics of the LFP signal examined in 7-s windows. Two characteristics were considered: a ratio of the cortical LFP power below 4 Hz and the power above 20 Hz and the kurtosis of the distribution of LFP values. The LFP was first decimated and low-pass filtered to 500 Hz. The distribution of power ratio values and kurtosis values for each 7-s window were fit with Gaussian mixture models. We used the power ratio to label windows of data as putative activated states if they were less than 1 standard deviation from the lower Gaussian's mean or they were labeled putative slow oscillation states if they were more than −1 standard deviation from the higher Gaussian's mean. We used the kurtosis values to label windows of data as putative activated states if they were >1 standard deviation from the higher Gaussian's mean or as putative slow oscillation states if they were <1 standard deviation from the lower Gaussian's mean. Any labels that agreed across the kurtosis-based labels and the power ratio-based labels were used as the final state assignments for those windows. Any windows that were unlabeled or did not agree across the two characteristics were ignored to conservatively reduce mistaken classifications. The raw LFP signals were plotted for visual inspection to assess the accuracy of labeling.

# **Detection of LC MUA Oscillations**

The LFP (digitized and stored at 24 kHz) recorded in the LC was bandpass filtered for high frequency, spiking activity (400–3,000 Hz) to obtain a multiunit spiking signal, as would be done typically for sorting single-unit spikes. The signal was

downsampled to 9 kHz. The signal was then rectified. This signal is termed the MUA signal. The power spectral density (PSD) of the MUA signal was obtained using a multitaper estimation generated from the Chronux toolbox in MATLAB (params.tapers = [3 5]). For each recording session (one per rat), the PSD of LC-MUA was calculated in 4-s windows. The resulting PSDs were k-means clustered. An optimal k was determined by a gap statistic. The mean PSD for each cluster was plotted and manually inspected for a 4- to 7-Hz peak. In some cases, multiple clusters of PSDs had a peak in the 4-7 Hz range with the only difference being the amplitude of the spectral peak. For each recording session, all clusters with 4-to 7-Hz peak were accepted as epochs with LC-MUA 5-Hz oscillations.

# **Cortical Spectrogram Calculation**

Cortical spectrograms, triggered on LC-MUA oscillation peaks, were calculated as follows. The LC-MUA signal was bandpass filtered at around a 5-Hz peak frequency (4–6 Hz) and Hilbert transformed to obtain the instantaneous phase. We selected peak times that occurred during the 4-s windows with 5-Hz oscillations (defined by PSD clustering, see METHODS section). A cortical spectrogram was generated for  $\pm 5\,\mathrm{s}$  around this peak using a complex Morelet wavelet transform. The large window was used to discount edge artifacts. The resulting analytic amplitudes were then cut to a small time around the oscillation. At each cortical frequency, the spectrogram was normalized as a Z-score. The normalization was done around each LC-MUA oscillation peak, then averaged across peaks for each rat. The presented spectrograms are the averages across rats.

# Coupling between LC-MUA Oscillation Phase and Cortical LFP Oscillation Amplitude

The phase-amplitude coupling was calculated using the LC-MUA signal as the oscillation for phase and the cortical LFP signal (downsampled to 9 kHz) as the oscillation for amplitude. The relationship between phase of one frequency and the amplitude of another frequency was quantified using the modulation index (MI), which is based on the Kullback-Leibler divergence of the circular distribution from uniformity (19). MI was calculated for each frequency pair (a frequency for phase,  $f_P$ , and a frequency for amplitude,  $f_A$ ). Only  $f_A$  that were two times  $f_P$  were considered, so that phase of at least two oscillation cycles was present for measuring the MI. We binned phase into 18 bins, where j is a bin, and then calculated the mean amplitude,  $\langle A_{f_A} \rangle$  of  $f_A$  in each phase bin of  $f_P$ . This resulted in a phase distribution of amplitudes,  $\langle A_{f_A} \rangle_{\theta_{f_P}(j)}$ . We normalized the distribution by dividing each bin by the sum across all bins. The resulting distribution is as follows:

$$P(j) = rac{\left\langle A_{f_A} 
ight
angle_{ heta_{f_P}(j)}}{\sum\limits_{k=1}^{N} \left\langle A_{f_A} 
ight
angle_{ heta_{f_P}(k)}},$$

where k is the phase bin and N is the total number of phase bins. The third step was to quantify the difference of this amplitude distribution from a uniform circular distribution. This was done using the Kullback–Leibler divergence. The

first step in calculating the divergence was to calculate the Shannon Entropy of P(j), which is as follows:

$$H(P) = -\sum_{j=1}^{N} P(j) \log [P(j)].$$

The second step was to calculate the Kullback–Leibler divergence of the amplitude distribution from a uniform distribution, which is related to Shannon Entropy as follows:

$$D(P, U) = \log(N) - H(P),$$

where U is the uniform circular distribution. Note that, if the amplitude distribution is flat and the amplitude of  $f_A$  is the same for all phase bins of  $f_P$ , then  $\log(N)$  is the maximal possible entropy in which P(j) = 1/N and phase is equally distributed across all bins, j. Accordingly, the Kullback–Leibler divergence is normalized by the maximal entropy,  $\log(N)$ , in which case a uniformly distributed P(j) that is not different from U will push the MI to 0. Otherwise, MI will range 0 to 1, with 1 indicating that oscillations of  $f_A$  exist in a single  $f_P(j)$ . The MI is thus,

$$\mathrm{MI}_{f_{A,f_P}} = \frac{D(P_{f_{A,f_P}},U)}{\log(N)}.$$

To control for chance modulation, we constructed a surrogate set of MI values to measure the level of coupling between  $f_A$  and  $f_P$  that could occur by chance. We shuffled  $f_A$  and then calculated a surrogate MI. We performed this procedure 100 times. A 99% confidence interval threshold was subtracted from the MI of the real data, such that values equal to or less than 0 were nonsignificant.

#### **PFC Single-Unit Spike Sorting**

Single-unit spike sorting was performed using MountainSort (20). Units were assessed for amplitude stability over time, a low proportion (<1 quarter of the shoulder of the auto-correlogram) of spikes in the  $\pm 1$  ms interval of the autocorrelogram, and cross-correlograms not indicative of recordings from the same unit split into multiple clusters.

# **Joint Perievent Time Histograms**

The joint perievent spike histogram was calculated in 10 ms bins to capture spiking synchronized across single units with enough temporal proximity to evoke postsynaptic effects on target neurons (21–23). The joint perievent time histograms were normalized by subtracting the top 5% value obtained by selecting random event times that were equivalent to the number of  $h_{\gamma}$  events. We plotted the coincidence histogram using the values along the  $\pm 30$  ms diagonal of the joint perievent time histogram. These values were chosen because the  $h_{\gamma}$  transients to which the histograms were aligned lasted  ${\sim}60$  ms.

# Statistical Analyses

Mean and standard error are reported for normally distributed data. Median and standard deviation are reported for data that were not normally distributed. The names of the statistical tests are reported in the results and includes the test statistic and P value. When results were significant, a post hoc power calculation was included.

Data were tested for normality using a Shapiro-Wilk test ( $\alpha$  = 0.05) and homogeneity of variance ( $\alpha$  = 0.05) using an F

test (vartest2 in MATLAB). A Wilcoxon–Mann–Whitney test was used for comparing two groups when data were not normally distributed, otherwise a t test was used. In cases where variance was inhomogeneous, we used Welch's t test. Effect sizes are reported as Cohen's D for analysis of two groups. Post hoc power was calculated with sampsizepwr in MATLAB. For circular data, uniformity was assessed using Rayleigh's test for circular uniformity ( $\alpha$  = 0.05) in the CircStat toolbox in MATLAB (24).

# RESULTS

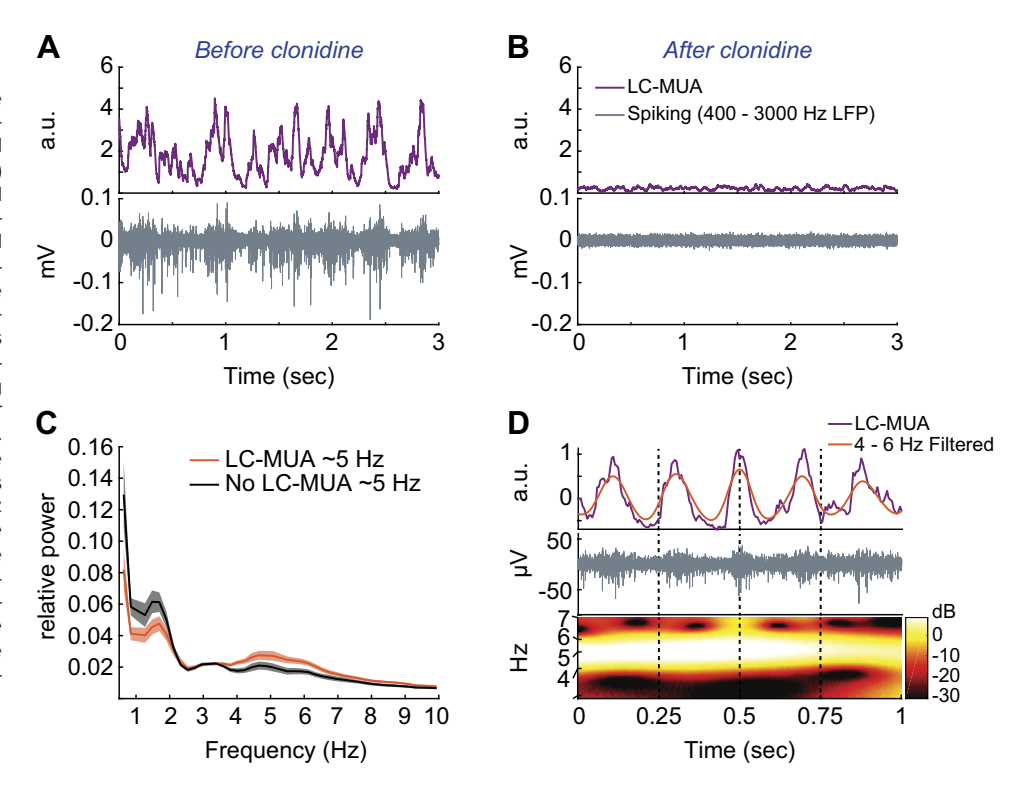
Our goal was to study the nature and directionality of LC-PFC interactions during epochs when LC population firing rate oscillated at 5 Hz. For this purpose, we used urethaneanesthetized rats, a common model for studying LC-PFC interactions (12, 14, 17, 18, 25, 26). We recorded wide-band (0.1–8 kHz) extracellular activity from deep layers of the prelimbic division of the rat PFC and from the LC core. LC-MUA was measured by first bandpass filtering (400 Hz to 3 kHz) to resolve extracellular spiking and then rectifying the signal. Figure 1A shows an example trace of bandpass filtered extracellular spiking signal (gray line) and the rectified LC-MUA signal (purple line). Large amplitude fluctuations in LC-MUA are generated primarily by action potentials produced by the neuronal population within 300 µm of the electrode (27, 28). This recording radius is comparable with the smallest dimension of LC core (29). Therefore, MUA was likely only capturing LC neuronal activity. We verified that the MUA originated from LC norephinephrine (NE)-containing neurons by injecting clonidine (0.05 mg/kg, ip) at the end of the recording session. Clonidine completely abolished the extracellular spiking that contributes to MUA signal in

all rats (an example rat is shown in Fig. 1*B*). Clonidine inhibits LC norepinephrine (NE) neurons by binding to  $\alpha$ -2 auto-inhibitory adrenoreceptors present on the soma and dendrites of LC-NE neurons (30). Clonidine administration discriminates extracellular unit spiking by LC-NE neurons from surrounding non-LC neurons because structures in the vicinity of the recording electrode do not have  $\alpha$ -2 receptors (31).

Consistent with an earlier report on LC-MUA (17), we confirmed that LC-MUA oscillates at both 1-2 Hz and 5 Hz during urethane anesthesia. We characterized LC-MUA oscillations by calculating the power spectral density (PSD) of the LC-MUA. For each recording session (n = 35 rats), we calculated the PSD in 4-s epochs and clustered them using principal components analysis and k-means clustering. Epochs with  $\sim$ 5-Hz oscillations of LC-MUA were identified as a cluster with a peak in the 4–7 Hz range. Figure 1C shows the average power spectrum of all 4-s data epochs with LC-MUA 5-Hz oscillations versus epochs without LC-MUA 5-Hz oscillations. Figure 1D shows an example clip of LC population rhythmic firing at 5 Hz. By examining the power of LC-MUA firing rate in 4-s windows, we reveal numerous epochs in which the recorded LC population activates and deactivates periodically every  $\sim$ 200 ms (i.e., at 5 cycles per s).

We next determined how LC single-unit firing rate fluctuated during LC-MUA 5-Hz oscillations. The oscillation cannot be detected in LC single units because units fire only  $\sim$ 1 Hz. We instead assessed the relationship between single-unit spike timing and the LC neuronal population oscillation. Nearly all single units (67.3% of 168 units) were significantly phase locked (Rayleigh's test for circular uniformity, P < 0.05) to the peak of the LC-MUA 5-Hz oscillation (i.e., the purple line in Fig. 1). Prior work has defined two types of LC

Figure 1. Multiunit activity (MUA) in the locus coeruleus (LC) exhibited rhythmic 5-Hz fluctuations. A: high-pass filtered (>400 Hz) extracellular activity (gray line) recorded from the LC. The band-limited power (purple line) was obtained by rectifying the 400-3,000 Hz bandpass-filtered signal. B: systemic administration of clonidine caused cessation of LC-MUA. C: the average LC-MUA power spectrum (normalized by total power) during epochs with and without LC-MUA  $\sim$ 5-Hz oscillations (n = 25 of 35 rats). Each 4-s recording epoch was classified as LC-MUA 5 Hz or non-5 Hz epoch and averaged within rat. The plots present the grand average across rats with standard error shown as shading. D: an example of LC-MUA 5-Hz oscillatory activity. The gray line is the high-pass filtered LC-MUA (>400 Hz). The purple line is the band limited power (purple line) of the 400-3,000 Hz bandpassfiltered signal, as in A and B. The orange line is the 4-6 Hz filtered LC-MUA. The wavelet transform of the purple line (LC-MUA) shows a clear 4- to 6-Hz oscillation.



single units, those with narrow waveforms and those with wide waveforms (18). About 52.6% of 76 narrow-type units and 79.3% of 92 wide-type units were phase locked to the LC-MUA 5-Hz oscillation. Thus, LC single units emit spikes as part of the LC neuronal population oscillating at 5 Hz. Given that 5-Hz oscillations are observable in only the LC-MUA signal, the remaining analyses focused on LC-MUA.

Prior research has demonstrated that slow (1-2 Hz) rhythmic LC activity occurs during sleep and anesthesia when the cortex is in a slow oscillation state in the same frequency range (14, 16-18, 26, 32) However, the brain state during which LC-MUA 5-Hz oscillations occur is not known. We assigned each 4-s recording epoch with LC-MUA 5-Hz oscillations to a "slow oscillation" or an "activated" cortical state (see MATERIALS AND METHODS for cortical state classification). The slow oscillation state consisted of periodically (1–2 Hz) alternating epochs of high and low neuronal excitability, whereas the "activated" state was one of continuously enhanced neuronal excitability (Fig. 2A). LC-MUA 5-Hz oscillations occurred mostly during the cortical activated state (Fig. 2B). Significantly more epochs of LC-MUA 5Hz were observed during the cortical activated state in comparison with the slow oscillation state ( $\chi^2 = 3,494.7$ , P < 0.0001). Having observed a brain state-dependency of LC-MUA 5-Hz oscillations, we focused the remaining analyses on the recording sessions with more than 40 s of LC-MUA 5-Hz oscillations in the activated cortical state. In total, 19 of 35 recording sessions had less than 40 s of LC-MUA 5-Hz oscillations and the cortical activity recorded in those rats consisted nearly entirely of the slow oscillation state (77.8% ± 8.1% of total recording time). In contrast, the 16 recording sessions with LC-MUA 5-Hz oscillations were in the cortical activated state for 74.3% ± 7.7% of the recording session.

# Frequency-Specific Modulation of the PFC Activity during LC Population Oscillations at ${\sim}5\,\text{Hz}$

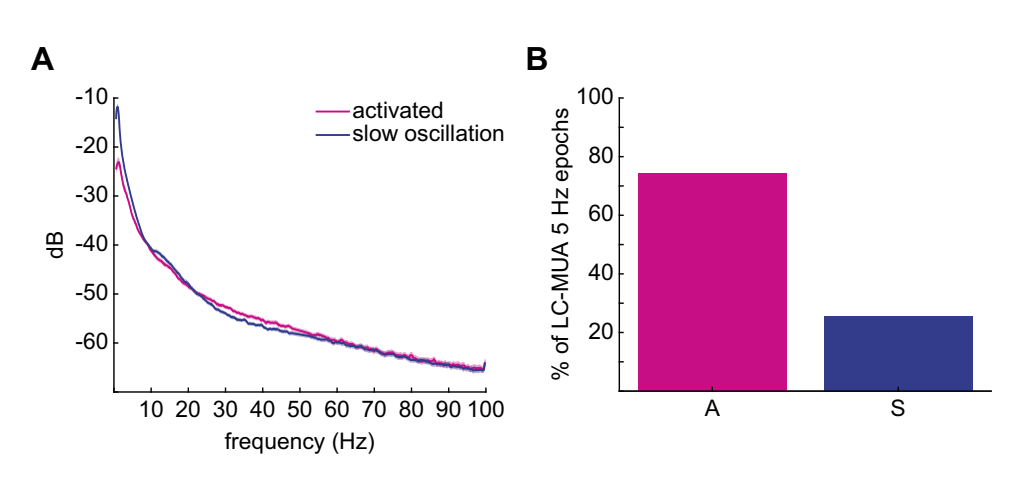
Although a phasic increase in LC-MUA has been proposed as a driver of the cortical activated state, the nature and directionality of LC-PFC interactions during epochs when LC population activity oscillates at 5 Hz have not yet been characterized. We first measured the relationship between the phase of LC-MUA 5-Hz oscillations (i.e., relative increases and decreases in LC population spike rate) and changes in

the power spectrum of the PFC LFP. This relationship was quantified using a modulation index (MI) that measured the nonuniformity of the phase distribution of PFC LFP amplitude between 30 Hz and 300 Hz (19). Following the method of Tort et al. (19), we subtracted the 99th largest MI value from 100 shuffled data sets, such that any MI values that are larger than zero are significant (one-sided permutation test, P < 0.01). Subtracting the 99% confidence intervals from the measured MI produces extremely small, yet significant MI values (typically,  $10^{-3}$ ). The values shown in Fig. 3A are similar to those reported in other studies (33–35). Moreover, LC-MUA 5-Hz oscillation peak-triggered cortical power spectra show a clear power modulation (Fig. 3B). This confirms the results of the MI analysis.

The MI analysis revealed that LC-MUA 5-Hz oscillations are associated with frequency band-specific modulation of PFC LFP power between 60 Hz and 200 Hz. This band includes high  $\gamma$  (h $\gamma$ ) as well as high-frequency oscillations (HFOs) (36-39). We will refer to this range  $(60-200 \,\mathrm{Hz})$  as the hγ band, although it also includes HFOs. Figure 3A shows the average MI value across all recording sessions in which LC-MUA 5-Hz oscillation epochs were present during the cortical activated state. Four of these rats lacked a clear modulation in the PFC power spectrum that was inconsistent with the population mean (especially in the frequencies higher than 250 Hz) and were excluded. The excluded data are shown with typical examples from individual rats in Supplemental Fig. S1 (https://figshare.com/s/56f03e7eabce0f2a6508). A boxplot illustrates the distribution, across rats, of the average MI value for 4–7 Hz phase with  $h_{\gamma}$  (60–200 Hz) amplitude (Fig. 3B). The temporal relationships between the PFC hy amplitude and LC-MUA 5-Hz oscillation phase are shown on PFC LFP power spectrograms triggered on the peaks of the LC-MUA 5-Hz oscillation (Fig. 3C). Consistent temporal relations between the LC-MUA rhythmic increases at 5 Hz and PFC LFP power increases exclusively in the hy band contrasts with prior work, demonstrating LC activation triggering a less specific (>30 Hz) change in PFC LFP (25, 26).

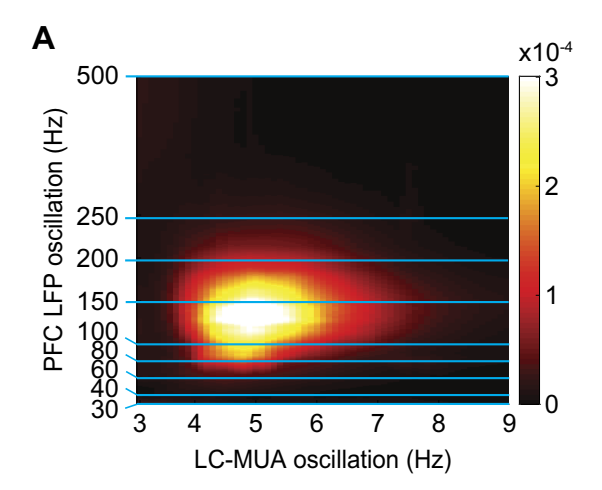
# The Directionality of the LC-PFC Interaction

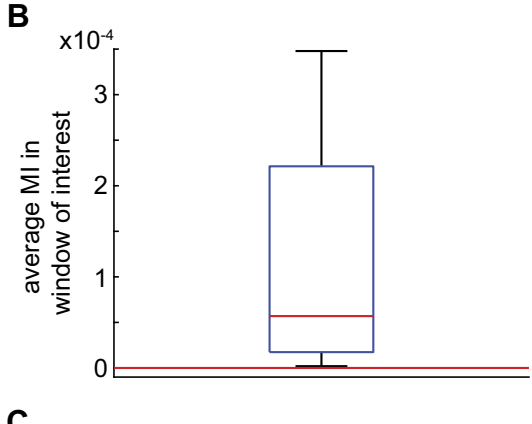
Having established that transient increases in PFC  $h\gamma$  power are phase-locked to LC-MUA 5-Hz oscillations, we turned to assessing the directionality of this interaction. The perievent spectrogram in Fig. 3C shows a PFC  $h\gamma$  power

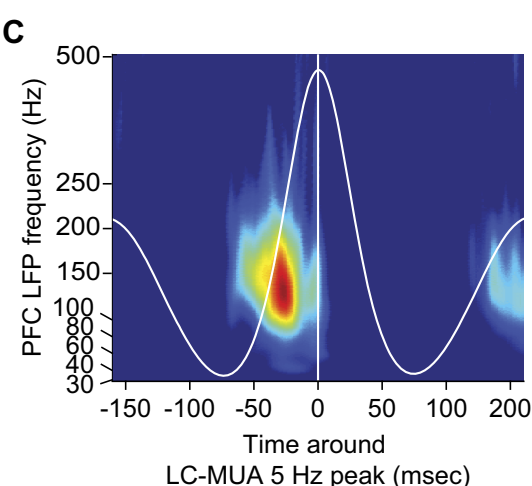


**Figure 2.** Locus coeruleus-multiunit activity (LC-MUA) 5-Hz oscillations occurred primarily in the activated cortical state. A: the prefrontal cortex (PFC) local field potential (LFP) power spectrum for the activated and slow oscillation states. The lines are the means across rats and the shading is the standard error. B: the percentage of LC-MUA 5-Hz epochs occurring in each cortical state.

change preceding the increase in LC-MUA activity, which suggests a directional interaction from the PFC to the LC. Indeed, the PFC can also exert both inhibitory and excitatory influences on LC activity (12, 14); however, interactions can also occur in the opposing direction given that the LC is an ascending neuromodulatory system that drives changes in the cortex (1–8). To infer the directionality of the LC-PFC interaction during epochs of LC-MUA 5-Hz oscillations, we used information theoretic measures to calculate the transfer entropy (TE) from the phase of the LC-MUA 5-Hz signal to the amplitude of the PFC LFP  $h_{\gamma}$  signal, as well as PFC to LC (40, 41). This measure quantifies the ability to predict the







current state of signal Y based on its past alone compared with when the past of signal X is included. For example, higher TE from X to Y would indicate that signal Y can be predicted from the past of signal X beyond what signal Y's self-history allows one to predict about its current state.

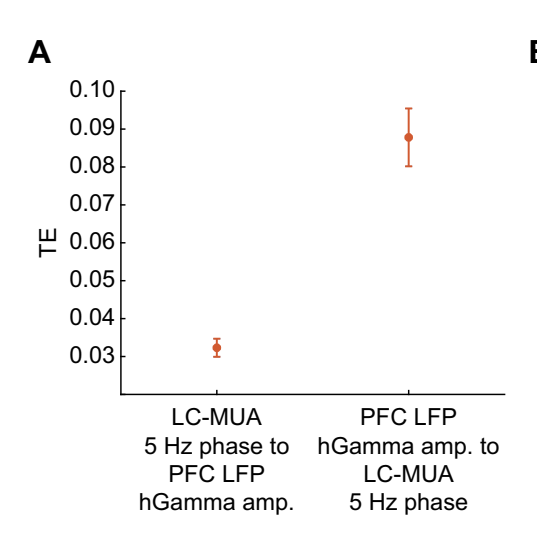
We observed that the direction of interaction during LC-MUA 5-Hz oscillations was actually predominantly from the PFC to the LC (Fig. 4A). Transfer entropy was larger from the past of the PFC LFP hy amplitude to present LC-MUA 5-Hz phase than vice versa (Wilcoxon rank-sum test, Z = 4.128, P =3.66E-5, power = 1.0, Cohen's D = 2.833). This result is consistent with the perievent spectrogram presented in Fig. 3C, which show the median latency from the PFC hγ power modulation to the LC-MUA 5-Hz oscillation peak is 29.1 ms (Fig. 4B). This delay after the  $h\gamma$  transient is consistent with the previously reported glutamatergic conduction time from the prelimbic division of the PFC to the LC in the rat (average 35 ms, range = 10-70 ms (12). The higher TE values from the PFC to the LC, as well as the consistency of the PFC h $\gamma$  to LC-MUA 5-Hz delay with the known conduction time from PFC to LC suggest that PFC h $\gamma$  transients may indicate the timing of the top-down excitatory input to LC.

The source of the cross-frequency LC-PFC interaction during epochs when the LC population oscillates at 5 Hz is unknown. However, the LFP signal, which reflects perisynaptic input around the electrode, did not have a 5-Hz oscillation in the PFC (Fig. 5). Therefore, it is unlikely that 5-Hz rhythmic synaptic input to the PFC is driving periodic changes in PFC activity, which, in turn, drive rhythmic changes in LC-MUA at 5 Hz. Accordingly, the synaptic and network events that drive this LC-PFC interaction to occur periodically at  $\sim\!\!200$  ms are, at present, unknown.

# The PFC Spike Rate during LC-PFC Interactions

The extracellular potential changes recorded in PFC as  $h\gamma$  oscillations are highly localized and cannot directly affect LC neurons; rather, it is the spiking output of PFC neurons that drives LC activity. We next assessed the spike rate of PFC units during LC-MUA 5-Hz oscillations. To assess how PFC spiking and  $h\gamma$  power relate to 5-Hz rhythmic fluctuations of LC-MUA, we aligned PFC multiunit spike rate to the peaks of

Figure 3. The phase of locus coeruleus-multiunit activity (LC-MUA) 5-Hz oscillations was associated with a frequency-specific (60-200 Hz) modulation of prefrontal cortex (PFC) local field potential (LFP). A: the average modulation index (MI) is plotted for each LC-MUA oscillation phase against PFC LFP oscillation amplitude. Zero values (black) are not significantly higher than those expected by chance (one-sided permutation test, P <0.01). B: the boxplot shows the distribution of MIs, across rats, in the window of interest (4- to 7-Hz phase, 60- to 200-Hz amplitude). For each rat, the values in this window of interest were not normally distributed (Shapiro-Wilk test) and the mean was influenced by very high values (i.e., the "hot spot" in A). As we wanted to quantify the magnitude of this hot spot across rats, we used the mean, rather than the median, to obtain a summary MI value for each rat. The boxplot shows the distribution of the MI hot spot magnitude across rats. Two outlier MIs (highly significant), which were 9.5E-4 and 5.4E-4, are not shown on the boxplot to allow visualization of the distribution of data. C: the PFC LFP power spectrogram is plotted aligned to the peak of LC-MUA 5-Hz oscillation. The spectrogram was first averaged across LC-MUA 5-Hz peaks and then averaged across rats. The white line shows LC-MUA (4-6 Hz filtered) aligned to peaks and averaged over all accepted sessions. The PFC LFP power is Z-score normalized within each frequency bin. The high  $\gamma$  (h $\gamma$ ) power increase preceding the peak of LC-MUA 5-Hz oscillation is apparent.



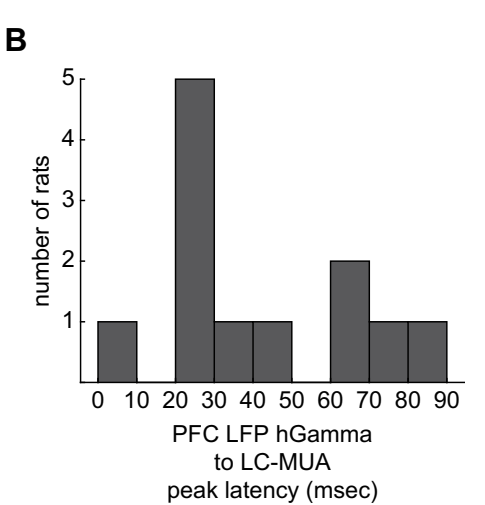


**Figure 4.** Prefrontal cortex (PFC) high  $\gamma$  (h $\gamma$ ; hGamma) amplitude is predictive of the future phase of locus coeruleus-multiunit activity (LC-MUA) 5-Hz oscillations. *A*: transfer entropy (TE) is higher in the direction from PFC h $\gamma$  amplitude to LC-MUA 5-Hz phase. The plot shows the mean and standard error of TE for each direction of interaction. *B*: a histogram showing the latency from the PFC local field potential (LFP) h $\gamma$  power peak until the LC-MUA 5-Hz oscillation peak for 12 rats. The median is 29.1 ms with a standard deviation of 25.7 ms and a range of -87.8 ms to -0.9 ms.

the LC-MUA 5-Hz oscillation. We highpass filtered the wideband PFC extracellular signal (at 500 Hz), detected spike times by thresholding the signal (3.5 standard deviations from the noise), and constructed a spike density function from those spike times using a 100 ms Gaussian kernel. We found that PFC MUA was modulated around LC-MUA 5-Hz oscillation peaks, albeit with a slight phase shift compared with PFC h $\gamma$  power (Fig. 6A).

Having demonstrated that both PFC spiking and PFC h $\gamma$  power cofluctuate around the peak of LC-MUA 5-Hz oscillations, we predicted that PFC single units would be phase-locked to LC-MUA 5-Hz oscillations. In four of the rats shown in Fig. 3, we used a 4-shank silicone probe (200  $\mu m$  between shanks) placed in the anterior-posterior plane within the PFC deep layers. These probes were chosen to isolate PFC single units. Each shank had two recording tetrodes separated by 500  $\mu m$  in the dorsal-ventral direction. Using these probes, we recorded 83 PFC single units (SE = 17 ± 2 units per rat, range = 9–22 units). Single-unit spike trains were converted to spike density functions using a 100-ms Gaussian

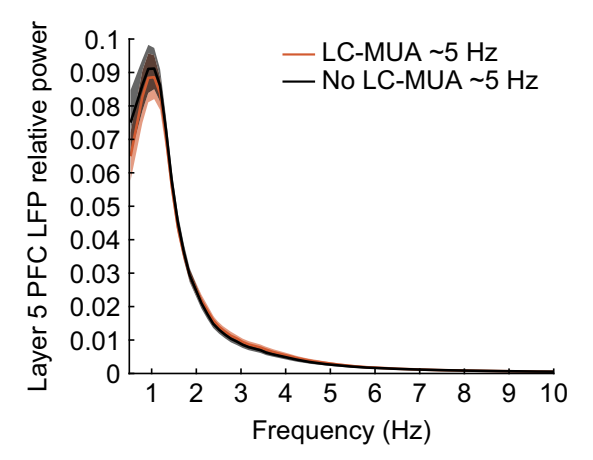


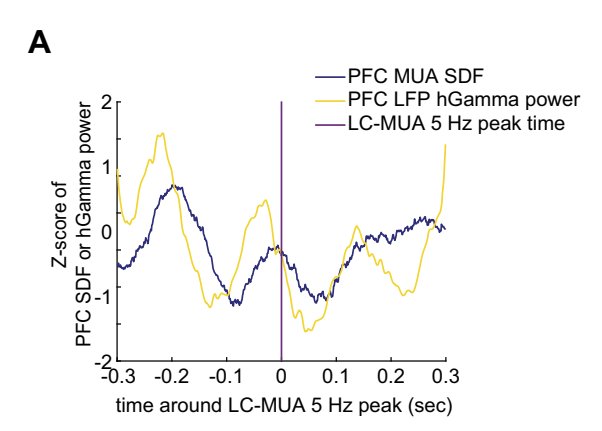
**Figure 5.** The prefrontal cortex (PFC) local field potential (LFP) spectrogram does not contain a peak at  $\sim$ 5 Hz. The power spectrum is plotted separately for epochs with (orange line) and without (black line) locus coeruleus-multiunit activity (LC-MUA) 5-Hz oscillations. Shading is the standard error around the mean.

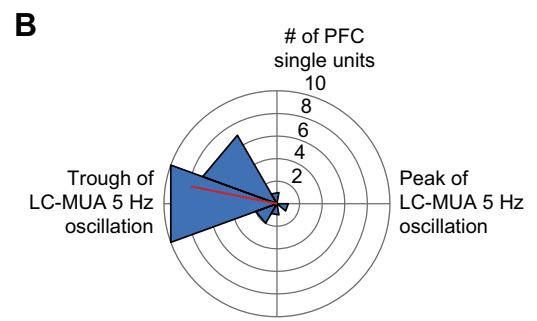
kernel. In line with this prediction, we found that 20 of 83 PFC single units (27%) were significantly phase-locked to LC-MUA 5-Hz oscillations (Rayleigh's test for circular uniformity, P < 0.05). The phase preference of these PFC units concentrated around the trough of the LC-MUA 5-Hz oscillation (Fig. 6B). The spike rate of the PFC single units, which were phase locked to LC-MUA 5-Hz oscillation, increased ~100 ms before the LC-MUA peak (Fig. 6C). This delay is inconsistent with the known conduction delays (~29 ms) from the PFC to the LC (12). Our findings suggest that the spiking of some PFC single units has a temporally consistent relationship with the LC-MUA 5-Hz oscillation, but that these spikes occur far earlier (~100 ms) in the LC-MUA oscillation cycle to monosynaptically drive its ascending phase given conduction delay of ~29 ms. Although polysynaptic influence of these PFC spikes on LC could not be ruled out, our sample of PFC units does not support the claim that PFC spike output monosynaptically drives the 5-Hz rhythmic firing in LC.

The role of PFC spikes phase locked to the trough of the LC-MUA 5-Hz oscillation remains unclear (Fig. 6B). The firing of a subset of PFC single units during the trough of the LC-MUA 5-Hz oscillation suggests that they may have a role in the rhythmic prefrontal-coeruleus interaction. One possibility is that an increase in PFC spiking ~100 ms before the LC-MUA peak is a local circuit mechanism that drives both the hy power increase and synchronous PFC spiking. We examined this possibility by calculating TE between PFC hy amplitude and PFC single units phase locked to LC-MUA 5-Hz oscillation (Fig. 7). We found that PFC spiking was predictive of the upcoming hγ power increase (Wilcoxon rank-sum test due to lack of normal distribution, Z = 2.61, P = 0.009, Cohen's D = 0.776, power = 0.736). The spiking of PFC units with no consistent relation to LC-MUA 5-Hz oscillation (Rayleigh's test for circular uniformity, P > 0.2) was not predictive of the hy power change (Wilcoxon rank-sum test, Z = 1.429, P = 0.153, Cohen's D = 0.343, power = 0.336).

# The PFC Unit-Pair Spike Synchrony during LC-PFC Interactions

Synchronous spiking between PFC neurons could be an alternative mechanism mediating the PFC effects on the LC.





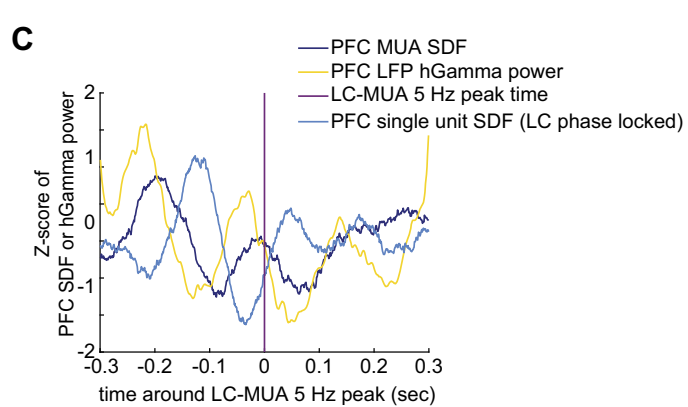


**Figure 6.** Prefrontal cortex (PFC) spiking is phase locked to locus coeruleus-multiunit activity (LC-MUA) 5-Hz oscillation. *A*: PFC single-unit and multiunit spike density functions (SDFs) and high  $\gamma$  (h $\gamma$ ; hGamma) amplitude cofluctuate around the LC-MUA 5-Hz peak (purple line). Values have been *Z*-scored to the means and standard deviation of the entire recording. *B*: spike timing of a subset of PFC single units (27%) is phase locked to the tough of the LC-MUA 5-Hz oscillation. The preferred phase is plotted for significantly phase-locked PFC units. The red line shows the circular mean across these phase-locked units. C: the same data are plotted, as in *A* with the addition of the average single-unit spike density function (SDF) for phase-locked PFC single units (dark blue line).

We tested the possibility that the increases in PFC  $h\gamma$  power are associated with a transient increase in synchronous spiking across PFC single units. We constructed joint perievent time histograms of PFC single-unit spiking using a ±60-ms window around PFC  $h\gamma$  transients (42, 43). This window was justified as a window that captured the entire duration of the  $h\gamma$  power increase. Figure 3*C* shows the power transient lasting  $\sim$ 60 ms. A ±60-ms window centered on the  $h\gamma$  power peak captures the entire  $h\gamma$  transient plus 30 ms of "baseline" on either side. This enabled us to test the hypothesis that PFC single unit pairwise synchrony increases during  $h\gamma$ 

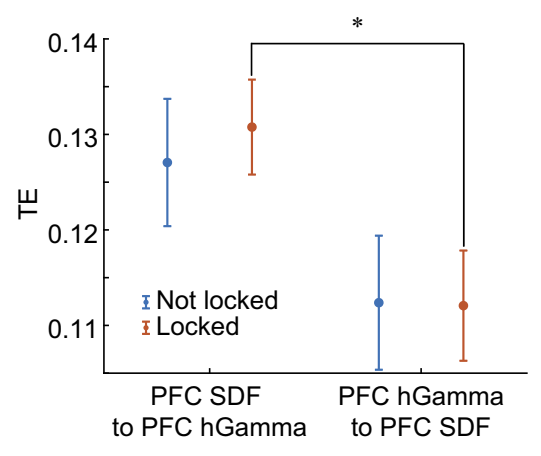


**Figure 7.** The spiking of prefrontal cortex (PFC) single units that are phase locked to locus coeruleus-multiunit activity (LC-MUA) 5-Hz oscillation predicts the local PFC high  $\gamma$  (h $\gamma$ ; hGamma) power increase. Transfer entropy (TE) between the PFC h $\gamma$  amplitude and PFC spike density function (SDF) was higher in the direction of the spiking to the h $\gamma$  signal. This directionality difference in TE was significant only for the units that were phase locked to LC activity. \*P < 0.01.

power transients. The diagonal of the joint perievent time histogram was used to calculate a coincidence histogram for each of the 808 pairs of PFC single units. The coincidence histograms serve to characterize synchronous spiking around the time of the h $\gamma$  transient (t = 0 in Fig. 8). We found an increase in synchrony around PFC h $\gamma$  power peaks in half (48%) of PFC single-unit pairs (Fig. 8). The synchronous spiking occurred  $\sim\!20$  ms before the h $\gamma$  power peak and lasted for  $\sim\!50$  ms. The h $\gamma$  power peak itself occurred  $\sim\!29$  ms before the LC-MUA 5-Hz peak, which means that synchronous PFC spiking transiently increased  $\sim\!49$  ms before the LC-MUA 5-Hz peak and lasted  $\sim\!21$  ms after the LC-MUA 5-Hz peak. PFC spikes occurring 20 ms after the h $\gamma$  peak are occurring during the descending phase of the LC-MUA 5-Hz oscillation. These spikes are occurring while LC-MUA is still elevated.

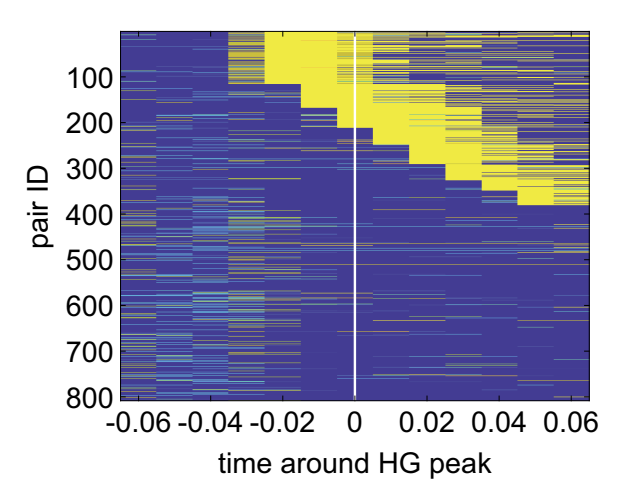


**Figure 8.** Prefrontal cortex (PFC) single-unit pair synchrony increases during PFC high  $\gamma$  (h $\gamma$ ; HG) transients. The coincident histograms of 808 PFC single-unit pairs (*y*-axis, sorted by synchrony onset time) show an increase in pairwise unit spike synchrony around PFC h $\gamma$  power peaks (*x*-axis). The coincident histograms are *Z*-scored with increases in synchrony (*Z*-score greater than 2) in yellow.

PFC spikes occurring up to 20 ms after the LC-MUA 5-Hz peak can still drive the elevated LC activity because the monosynaptic spike conduction time from PFC to LC is as fast as 10 ms for some PFC units. These data suggest a potential mechanism for PFC monosynaptic control over LC firing using transiently synchronous spiking during  $h_{\gamma}$  transients. However, it is important to note that the recorded PFC single units may or may not project to the LC. In summary, it appears that the subset of PFC neurons that spike during the troughs of LC-MUA 5-Hz oscillations may drive local hy transients, which are themselves related to the synchronous spiking of PFC units that may drive the LC-MUA increase.

### DISCUSSION

In this study, we examined the relationship between rhythmic (5 Hz) increases in LC-MUA and neural activity in the PFC, an important forebrain target of LC. In contrast to the welldescribed slower (1-2 Hz) rhythmic increases in LC spiking that are observed during cortical slow oscillations (16-18), the LC-MUA 5-Hz oscillations predominantly occurred during the activated cortical state devoid of cortical slow oscillations. By measuring cross-frequency coupling between LC-MUA oscillations within 1-10 Hz range and the power spectrum of PFC LFP (30-500 Hz), we observed a systematic temporal relationship between the phase of LC-MUA oscillations within a 4-6 Hz range and PFC hy power (60–200 Hz). The transient increase in PFC hy power preceded the LC-MUA 5-Hz oscillation peak by  $\sim$ 29 ms. This time lag is consistent with the previously reported orthodromic conduction times from deep layers of the prelimbic division of the PFC in rats (12). Furthermore, using transfer entropy, we show that PFC  $h\gamma$  power is temporally predictive of LC-MUA 5-Hz phase. The transfer entropy and the biologically plausible delay time are each evidence for the idea that PFC hy transients may indicate the timing of the top-down excitatory input to LC, at least under conditions when LC neuronal population activity fluctuates rhythmically at 5 Hz.

Hγ transients are unlikely to have a direct synaptic effect on LC neurons because they are highly local. We showed that synchronous spiking between PFC single units occurs during hy transients and reached maximum around the peak of LC-MUA 5-Hz oscillation. We suggest that this increased population synchrony in PFC may be top-down excitatory input to LC. The timing between synchronous PFC spiking and the peak of the LC-MUA oscillation is consistent with the conduction velocity of the prefrontal-coeruleus projection. Synchronous spiking is an ideal candidate for top-down glutamatergic control over LC neurons because glutamatergic neurons spiking within  $\sim$ 5 ms of one another evoke a larger postsynaptic response (21-23). Collectively, our findings suggest that the PFC hy transients and, critically, associated neuronal spike synchrony may be a sign of PFC top-down control over LC population activity.

We also observed a subpopulation of PFC single units ( $\sim$ 27%) that increased their firing rate  $\sim$ 100 ms before the peak of LC-MUA 5-Hz oscillation. Given the conduction velocity of the prefrontal-coeruleus projection, these spikes are unlikely to monosynaptically drive LC-MUA. However, their consistent timing in relation to the trough of LC-MUA 5-Hz oscillation suggested that these spikes are involved in the prefrontal-coerulear interaction. Transfer entropy analysis revealed that the spikes of these PFC neurons were predictive of the upcoming change in PFC hy power. Therefore, a subset of PFC single units that are phase locked to the trough of the LC-MUA 5-Hz oscillation (thus preceding the hγ power increase) may drive the  $h_{\gamma}$  transient and the associated synchronized spiking in PFC. It also cannot be excluded that PFC spikes consistently occurring ~100 ms before the LC-MUA peak could drive LC-MUA directly via multiple polysynaptic routes.

Overall, we propose that a local PFC circuit mechanism drives the synchronous spiking that influences LC-MUA (Fig. 9). Notably, most (67.3%), but not all LC single units spiked as part of the LC population firing rate oscillation at

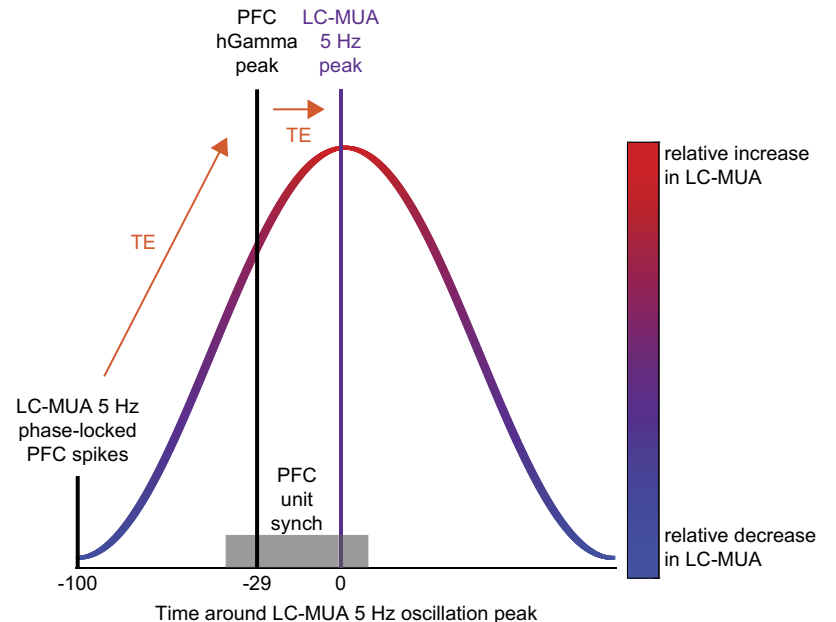


Figure 9. A putative model of top-down prefrontal control over the locus coeruleus (LC). We found that prefrontal cortex (PFC) spikes were phase locked to the trough of LC-multiunit activity (MUA) 5-Hz oscillation. Given the 10- to 70-ms conduction time from the PFC to the LC, this time point is too early to conduct a signal that could evoke an increase in LC-MUA spike rate (red part of the oscillation). Instead, these PFC spikes were predictive of a local high  $\gamma$  (hy; hGamma) power increase (orange arrow, direction of transfer entropy, TE). This hy transient was, in turn, predictive of the subsequently increased LC-MUA (red peak). Data are shown in Fig. 4A. The  $h\gamma$  transient precedes the LC-MUA peak by 29 ms. Data are shown in Fig. 3C and Fig. 4B. In a window of  $-20\ \text{ms}$  to  $+\,50\ \text{ms}$  around the  $h\gamma$  peak (or -49ms to +21 ms around the LC-MUA peak), PFC single-unit pairs spike with transiently increased synchrony (gray area on x-axis). Data are shown in Fig. 8. A chain of neural events from the PFC spikes time locked to the through of LC-MUA 5-Hz oscillation to  $h\gamma$ -associated spike synchrony in the PFC may drive an increase in LC spike rate.

5 Hz; these nonparticipating LC neurons may be unresponsive to this type of PFC interaction and thus illustrate potential heterogeneity of the LC neuronal population. It remains to be determined how the 5 Hz rhythmicity in the LC emerges and if it is specific to anesthesia or has functional significance in behaving animals.

# ACKNOWLEDGMENTS

We thank Prof. Stefano Panzeri and Dr. Michel Besserve for help in implementing the transfer entropy analysis in MATLAB. We are grateful to Drs. Antonio Fernández-Ruiz and Martin Vinck for comments on the manuscript.

### GRANTS

This research was supported by European Union FP7 funding as a Marie Curie Fellowship to N.K.T. (PIIF-GA-2012-331122) and Future and Emerging Technologies (FET) Open funding to S.P., O.E., and N.K.L. [Towards new Brain-Machine Interfaces: State-dependent information coding (SICODE)].

# DISCLOSURES

No conflicts of interest, financial or otherwise, are declared by the authors.

# AUTHOR CONTRIBUTIONS

N.K.T., N.K.L., and O.E. conceived and designed research; N.K.T. performed experiments; N.K.T. analyzed data; N.K.T. and O.E. interpreted results of experiments; N.K.T. prepared figures; N.K.T. drafted manuscript; N.K.T., N.K.L., and O.E. edited and revised manuscript; N.K.T., N.K.L., and O.E. approved final version of manuscript.

# REFERENCES

- Fallon JH, Koziell DA, Moore RY. Catecholamine innervation of the basal forebrain. II. Amygdala, suprarhinal cortex and entorhinal cortex. J Comp Neurol 180: 509–532, 1978. doi:10.1002/cne.901800308.
- Grzanna R, Morrison JH, Coyle JT, Molliver ME. The immunohistochemical demonstration of noradrenergic neurons in the rat brain: the use of homologous antiserum to dopamine-beta-hydroxylase. Neurosci Lett 4: 127–134, 1977. doi:10.1016/0304-3940(77)90127-6.
- Kebschull JM, Silva PD, Reid AP, Peikon ID, Albeanu DF, Zador AM. High-throughput mapping of single-neuron projections by sequencing of barcoded RNA. Neuron 91: 975–987, 2016. doi:10.1016/j.neuron.2016.07.036.
- Loughlin SE, Foote SL, Fallon JH. Locus coeruleus projections to cortex: topography, morphology and collateralization. *Brain Res Bull* 9: 287–294, 1982. doi:10.1016/0361-9230(82)90142-3.
- Morrison JH, Molliver ME, Grzanna R. Noradrenergic innervation of cerebral cortex: widespread effects of local cortical lesions. *Science* 205: 313–316, 1979. doi:10.1126/science.451605.
- Schwarz LA, Miyamichi K, Gao XJ, Beier KT, Weissbourd B, DeLoach KE, Ren J, Ibanes S, Malenka RC, Kremer EJ, Luo L. Viralgenetic tracing of the input-output organization of a central noradrenaline circuit. Nature 524: 88–92. 2015. doi:10.1038/nature14600.
- Swanson LW, Hartman BK. The central adrenergic system. An immunofluorescence study of the location of cell bodies and their efferent connections in the rat utilizing dopamine-beta-hydroxylase as a marker. *J Comp Neurol* 163: 467–505, 1975. doi:10.1002/cne.901630406.
- Waterhouse BD, Lin CS, Burne RA, Woodward DJ. The distribution of neocortical projection neurons in the locus coeruleus. *J Comp Neurol* 217: 418–431, 1983. doi:10.1002/cne.902170406.
- Arnsten AFT, Goldman-Rakic PS. Selective prefrontal cortical projections to the region of the locus coeruleus and raphe nuclei in the

- rhesus monkey. *Brain Res* 306: 9–18, 1984. doi:10.1016/0006-8993 (84)90351-2.
- Aston-Jones G, Cohen JD. Adaptive gain and the role of the locus coeruleus-norepinephrine system in optimal performance. *J Comp Neurol* 493: 99–110, 2005. doi:10.1002/cne.20723.
- Breton-Provencher V, Sur M. Active control of arousal by a locus coeruleus GABAergic circuit. Nat Neurosci 22: 218–228, 2019. doi:10.1038/s41593-018-0305-z.
- Jodo E, Chiang C, Aston-Jones G. Potent excitatory influence of prefrontal cortex activity on noradrenergic locus coeruleus neurons. Neuroscience 83: 63–79, 1998. doi:10.1016/s0306-4522(97)00372-2.
- Luppi P-H, Aston-Jones G, Akaoka H, Chouvet G, Jouvet M. Afferent projections to the rat locus coeruleus demonstrated by retrograde and anterograde tracing with cholera-toxin B subunit and *Phaseolus vulgaris* leucoagglutinin. *Neuroscience* 65: 119–160, 1995. doi:10.1016/0306-4522(94)00481-j.
- Sara SJ, Hervé-Minvielle A. Inhibitory influence of frontal cortex on locus coeruleus neurons. *Proc Natl Acad Sci USA* 92: 6032–6036, 1995. doi:10.1073/pnas.92.13.6032.
- Sesack SR, Deutch AY, Roth RH, Bunney BS. Topographical organization of the efferent projections of the medial prefrontal cortex in the rat: an anterograde tract-tracing study with phaseolus vulgaris leucoagglutinin. *J Comp Neurol* 290: 213–242, 1989. doi:10.1002/cne 902900205
- Eschenko O, Magri C, Panzeri S, Sara SJ. Noradrenergic neurons of the locus coeruleus are phase locked to cortical up-down states during sleep. Cereb Cortex 22: 426–435, 2012. doi:10.1093/cercor/bhr121.
- Safaai H, Neves R, Eschenko O, Logothetis NK, Panzeri S. Modeling the effect of locus coeruleus firing on cortical state dynamics and single-trial sensory processing. *Proc Natl Acad Sci USA* 112: 12834–12839, 2015. doi:10.1073/pnas.1516539112.
- Totah NK, Neves RM, Panzeri S, Logothetis NK, Eschenko O. The locus coeruleus is a complex and differentiated neuromodulatory system. Neuron 99: 1055–1068.e6, 2018. doi:10.1016/j.neuron.2018.07.037.
- Tort ABL, Komorowski R, Eichenbaum H, Kopell N. Measuring phase-amplitude coupling between neuronal oscillations of different frequencies. J Neurophysiol 104: 1195–1210, 2010 [Erratum in J Neurophysiol 104: 2302, 2010]. doi:10.1152/jn.00106.2010.
- Chung JE, Magland JF, Barnett AH, Tolosa VM, Tooker AC, Lee KY, Shah KG, Felix SH, Frank LM, Greengard LF. A fully automated approach to spike sorting. *Neuron* 95: 1381–1394.e6, 2017. doi:10.1016/j.neuron.2017.08.030.
- Abeles M. Role of the cortical neuron: integrator or coincidence detector? Isr J Med Sci 18: 83–92, 1982.
- Alonso J-M, Usrey WM, Reid RC. Precisely correlated firing in cells of the lateral geniculate nucleus. *Nature* 383: 815–819, 1996. doi:10.1038/383815a0.
- Fujisawa S, Amarasingham A, Harrison MT, Buzsáki G. Behaviordependent short-term assembly dynamics in the medial prefrontal cortex. *Nat Neurosci* 11: 823–833, 2008. doi:10.1038/nn.2134.
- Berens P. CircStat: a MATLAB toolbox for circular statistics. J Stat Softw 31: 1–21, 2009. doi:10.18637/jss.v031.i10.
- Marzo A, Totah NK, Neves RM, Logothetis NK, Eschenko O. Unilateral electrical stimulation of rat locus coeruleus elicits bilateral response of norepinephrine neurons and sustained activation of medial prefrontal cortex. *J Neurophysiol* 111: 2570–2588, 2014. doi:10.1152/jn.00920.2013.
- Neves RM, Keulen S, van Yang M, Logothetis NK, Eschenko O. Locus coeruleus phasic discharge is essential for stimulus-induced gamma oscillations in the prefrontal cortex. *J Neurophysiol* 119: 904–920, 2018. doi:10.1152/jn.00552.2017.
- Logothetis NK. The underpinnings of the BOLD functional magnetic resonance imaging signal. *J Neurosci* 23: 3963–3971, 2003. doi:10.1523/JNEUROSCI.23-10-03963.2003.
- Logothetis NK. What we can do and what we cannot do with fMRI. Nature 453: 869–878, 2008. doi:10.1038/nature06976.
- Grzanna R, Molliver ME. The locus coeruleus in the rat: an immunohistochemical delineation. Neuroscience 5: 21–40, 1980. doi:10.1016/ 0306-4522(80)90068-8.
- Aghajanian GK, Cedarbaum JM, Wang RY. Evidence for norepinephrine-mediated collateral inhibition of locus coeruleus neurons. Brain Res 136: 570–577, 1977. doi:10.1016/0006-8993(77)90083-x.

- McCune SK, Voigt MM, Hill JM. Expression of multiple alpha adrenergic receptor subtype messenger RNAs in the adult rat brain. Neuroscience 57: 143–151, 1993. doi:10.1016/0306-4522(93)90116-W.
- Lestienne R, Hervé-Minvielle A, Robinson D, Briois L, Sara SJ. Slow oscillations as a probe of the dynamics of the locus coeruleusfrontal cortex interaction in anesthetized rats. *J Physiol Paris* 91: 273–284, 1997. doi:10.1016/S0928-4257(97)82407-2.
- Amadei EA, Johnson ZV, Kwon YJ, Shpiner AC, Saravanan V, Mays WD, Ryan SJ, Walum H, Rainnie DG, Young LJ, Liu RC. Dynamic corticostriatal activity biases social bonding in monogamous female prairie voles. *Nature* 546: 297–301, 2017. doi:10.1038/nature22381.
- Park H-D, Barnoud C, Trang H, Kannape OA, Schaller K, Blanke O. Breathing is coupled with voluntary action and the cortical readiness potential. Nat Commun 11: 289, 2020. doi:10.1038/s41467-019-13967-9.
- Spaak E, Bonnefond M, Maier A, Leopold DA, Jensen O. Layer-specific entrainment of γ-band neural activity by the α rhythm in monkey visual cortex. Curr Biol 22: 2313–2318, 2012. doi:10.1016/j.cub.2012.10.020.
- Ray S, Crone NE, Niebur E, Franaszczuk PJ, Hsiao SS. Neural correlates of high-gamma oscillations (60-200 Hz) in macaque local field potentials and their potential implications in electrocorticography. *J Neurosci* 28: 11526–11536, 2008. doi:10.1523/JNEUROSCI.2848-08.2008.

- Ray S, Niebur E, Hsiao SS, Sinai A, Crone NE. High-frequency gamma activity (80–150Hz) is increased in human cortex during selective attention. *Clin Neurophysiol* 119: 116–133, 2008. doi:10.1016/j.clinph.2007.09.136.
- Ray S, Maunsell JHR. Different origins of gamma rhythm and highgamma activity in macaque visual cortex. *PLoS Biol* 9: e1000610, 2011. doi:10.1371/journal.pbio.1000610.
- Khodagholy D, Gelinas JN, Buzsáki G. Learning-enhanced coupling between ripple oscillations in association cortices and hippocampus. Science 358: 369–372, 2017. doi:10.1126/science.aan6203
- Besserve M, Schölkopf B, Logothetis NK, Panzeri S. Causal relationships between frequency bands of extracellular signals in visual cortex revealed by an information theoretic analysis. *J Comput Neurosci* 29: 547–566, 2010. doi:10.1007/s10827-010-0236-5.
- Besserve M, Lowe SC, Logothetis NK, Schölkopf B, Panzeri S. Shifts of gamma phase across primary visual cortical sites reflect dynamic stimulus-modulated information transfer. *PLoS Biol* 13: e1002257, 2015. doi:10.1371/journal.pbio.1002257.
- Aertsen AM, Gerstein GL, Habib MK, Palm G. Dynamics of neuronal firing correlation: modulation of "effective connectivity". J Neurophysiol 61: 900–917, 1989. doi:10.1152/jn.1989.61.5.900.
- 43. **Brody CD.** Correlations without synchrony. *Neural Comput* 11: 1537–1551, 1999. doi:10.1162/089976699300016133.